

## Multi-phase gas nature in the sub-pc region of the active galactic nuclei II: Optical-UV spectra originated in the ionized gas

KEIICHI WADA,<sup>1,2,3</sup> YUKI KUDOH,<sup>1</sup> AND TOHRU NAGAO<sup>2</sup>

<sup>1</sup>*Kagoshima University, Graduate School of Science and Engineering, Kagoshima 890-0065, Japan*

<sup>2</sup>*Ehime University, Research Center for Space and Cosmic Evolution, Matsuyama 790-8577, Japan*

<sup>3</sup>*Hokkaido University, Faculty of Science, Sapporo 060-0810, Japan*

### ABSTRACT

Through two-dimensional radiation-hydrodynamical simulations, we investigate the spectral properties of ionized gas irradiated by an active galactic nucleus with a supermassive black hole of  $10^7 M_{\odot}$ . For the gas inside the dust-sublimation radius ( $r \sim 10^{-2}$  pc), we conduct post-process pseudo-three-dimensional calculations utilizing the spectral synthesis code CLOUDY. We show that we can reproduce various broad emission lines in optical and ultraviolet wavelengths. The line profiles change depending on the viewing angles even for a small range from the rational axis, i.e., 5-30 degrees; most lines, such as H $\alpha$ , are characterized by a double-peaked profile, reflecting that the emissions are originated in the surface of the rotating disk. By contrast, high-ionization emission lines such as C iv  $\lambda 1549$  show a double-peaked profile for a nearly face-on view, as these lines derive from the fast outflowing gas from the disk surface. Our results suggest that some properties of the bright UV-optical emission lines observed in Seyfert-like AGNs can be caused by the radiation-driven fountain flow inside the dust sublimation radius.

### 1. INTRODUCTION

Type 1 active galactic nuclei (AGNs) are characterized by broad ( $\gtrsim 1000$  km s<sup>-1</sup>) emission lines. These include Balmer lines, C iv  $\lambda 1549$ , and Mg ii  $\lambda 2798$ . (e.g., Osterbrock & Mathews 1986; Peterson 1997). These lines most likely originate in the photoionized gas derived from the strong radiation emitted by the AGN (e.g. Osterbrock & Ferland 2006; Netzer 2013). The widths of the individual emission lines have often been used to estimate central black hole (BH) mass (e.g., Ferrarese & Ford 2005; Bentz et al. 2009). However, for a reliable estimate of the masses of supermassive BHs, understanding the geometry and kinematics of broad emission line regions (BLRs) and their origins is essential. In terms of low-ionization gas, BLRs are

believed to originate in a rotating disk, but radial motions such as outflows and inflows are also assumed to be present (e.g., Gaskell 1982; Smith & Raine 1985; Ferland & Persson 1989; Chiang & Murray 1996a; Gaskell 2009, and references therein).

Recently, the spatial structures of BLRs were partially resolved using a near-infrared interferometer in some nearby AGNs (GRAVITY Collaboration et al. 2018, 2020, 2021). The results are consistent with the size determined by the reverberation mapping (RM) technique (e.g., Blandford & McKee 1982; Peterson et al. 1993, 2004; Lawther et al. 2018; Baskin & Laor 2018). The outer edge of the BLR is  $\sim 1/3$  of the dust sublimation radius (Netzer & Laor 1993; Suganuma et al. 2006; Netzer 2015, 2020; GRAVITY Collaboration et al. 2022). The velocity-resolved RM (e.g., Barth et al. 2011; Almeyda et al. 2020) can provide clues about the spatial distribution of BLRs in Seyfert 1 galaxies, such as NGC 5548 (Williams et al. 2020). However, it is still unclear whether these two components are or are not physically related.

If BLR is extended to the inner edge of the dust torus, the structure and dynamics of the dust sublimation region are critical in understanding the origins of BLRs (Baskin & Laor 2018). The failed radiatively accelerated dusty outflow (FRADO) is a type of dynamical model (Czerny & Hryniewicz 2010; Naddaf et al. 2021), but the multi-dimensional dynamics of dusty gas, which are essential for the line shape and distribution of ionized gas, is not directly solved in the FRADO model (see also Dorodnitsyn & Kallman 2021).

BLR gases are often assumed to be high-density ( $\sim 10^{10} - 10^{11} \text{ cm s}^{-3}$ ) cloudlets. However, the realistic structures and dynamics of BLR “clouds” remain theoretically unclear. Recently, Matthews et al. (2020) demonstrated that biconical disk winds illuminated by an AGN continuum can produce BLR-like spectra. Based on a simple clumpy wind model, they conducted Monte Carlo radiation transfer calculations, and found that broad emission lines with equivalent widths and line ratios comparable to those observed in quasars. Although they have succeeded in reproducing spectra resembling those of luminous, type-1 AGNs, their model needs to assume wind properties and geometry with various free parameters. As they pointed out in the summary of the paper, the radiative transfer calculations based on hydrodynamic simulations are necessary for the next step.

The hydrodynamics of dusty gas under central radiation was recently studied in terms of the “obscuring torus” on a 1–10 pc scale (Wada 2012; Dorodnitsyn et al. 2012; Wada 2015; Namekata & Umemura 2016; Williamson et al. 2020). Multi-dimensional radiation-hydrodynamic calculations previously revealed that outflowing multi-phase gas with dust is formed naturally, and the Type 1 and 2 dichotomies in the spectral energy distribution (SED) can thus be naturally explained (Schartmann et al. 2014). This dynamical model (“radiation-driven fountain”) effectively explains the multi-wavelength observations of the nearby Type 2 Seyfert galaxy, the Circinus galaxy, in many aspects: molecular and atomic emission and absorption lines in the central 10 pc (Izumi et al. 2018; Wada et al. 2018a; Uzuo et al. 2021; Matsumoto

et al. 2022; Izumi & Wada 2023), the conical shape and line ratio properties of the narrow emission line region (e.g., [OIII]  $\lambda$  5007 (Wada et al. 2018b)), and the X-ray spectral energy distribution and lines (Buchner et al. 2021; Ogawa et al. 2022).

As the second paper of the series, we here focus on emission lines derived from the gas inside the dust-sublimation radius ( $< 0.02$  pc) using a high-spatial-resolution radiation-driven fountain model (Kudoh et al. 2023) (hereafter Paper I). In contrast to Matthews et al. (2020), we investigate gas dynamics in relatively low luminosity AGNs with a moderate black hole (BH) mass, i.e.,  $10^7 M_\odot$  in this paper. This is partly because a larger dynamic range should be necessary for more luminous quasar-type AGNs associated with more massive BHs, and the radiation-driven fountain scheme is most relevant to explain the multi-wavelength properties of Seyfert-type AGNs (e.g., Izumi & Wada 2023).

Following Wada et al. (2018b), we analyze a snapshot of the hydrodynamic simulation using the photo-ionized code CLOUDY (Ferland et al. 2017). The line profiles of the hydrogen recombination lines as well as the high-ionization lines are discussed. This is an attempt to understand the origins of the emission lines of AGNs based on a physics-motivated multi-dimensional model.

## 2. NUMERICAL METHODS

### 2.1. Physical model in gas, dust, and radiation

We use one-snapshot data from a two-dimensional radiation-hydrodynamic simulation in a quasi-steady state (see Paper I in detail) and calculate the radiative-transfer as a post process (see §2.2). Here, we briefly summarize the hydrodynamic model.

We solve the evolution of a dusty gas disk with mass inflow irradiated by a central source in a computational box of  $r = 10^{-4} \sim 50$  pc (Figure 1). This is an extension of the three-dimensional radiation-driven fountain simulations (Wada 2012, 2015) with a higher resolution. However, we assume an axisymmetric distribution using a cylindrical coordinate. The included physics here are those of radiative heating by X-ray as well as the radiation force that induces both dusty and ionized gases. The black hole mass is  $M_{\text{BH}} = 10^7 M_\odot$  and the Eddington ratio is 0.1 (the bolometric luminosity is  $1.25 \times 10^{44}$  erg s $^{-1}$ ).

The basic equations are

$$\frac{\partial \rho}{\partial t} + \nabla \cdot [\rho \mathbf{v}] = 0, \quad (1)$$

$$\frac{\partial \rho \mathbf{v}}{\partial t} + \nabla \cdot [\rho \mathbf{v} \mathbf{v} + P_g \mathbf{I}] = \mathbf{f}_{\text{rad}} + \mathbf{f}_{\text{grav}} + \mathbf{f}_{\text{vis}}, \quad (2)$$

$$\begin{aligned} \frac{\partial e}{\partial t} + \nabla \cdot [(e + P_g) \mathbf{v}] = & -\rho \mathcal{L} + \mathbf{v} \cdot \mathbf{f}_{\text{rad}} + \\ & \mathbf{v} \cdot \mathbf{f}_{\text{grav}} + W_{\text{vis}}, \end{aligned} \quad (3)$$

where total energy density is  $e = P_g/(\gamma - 1) + \rho v^2/2$ , and the specific heat ratio adiabatically, i.e.  $\gamma = 5/3$ .  $\mathcal{L}$  is the net heating/cooling rate per unit mass. We adopted the gravitational force,  $\mathbf{f}_{\text{grav}} = -\rho G M_{\text{BH}} \mathbf{e}_r / r^2$ , where  $G$  denotes the gravitational constant and  $r = \sqrt{R^2 + z^2}$  is the distance from the center of BH with  $M_{\text{BH}} = 10^7 M_{\odot}$ . The radiation force is  $\mathbf{f}_{\text{rad}} \simeq \int \nabla \cdot F_{\nu} \mathbf{e}_r d\nu$ , where  $F_{\nu}$  is the radiation flux.

We assume the  $\alpha$  viscosity ( $\alpha = 0.1$ ) to achieve mass accretion through the disk as  $\nu_{\text{vis}} = \alpha c_s^2 / \Omega_K$  with the viscosity depends on the sound speed  $c_s$  and the Keplerian angular speed  $\Omega_K$  (Shakura & Sunyaev 1973). The viscous force in Equation (2) and the viscous heating in Equation 4 are taken from Ohsuga et al. (2005):

$$\mathbf{f}_{\text{vis}} \equiv \frac{\mathbf{e}_{\varphi}}{R^2} \frac{\partial}{\partial R} \left[ R^2 \alpha P_g \frac{R^2}{v_{\varphi}} \frac{\partial}{\partial R} \left( \frac{v_{\varphi}}{R} \right) \right], \quad (4)$$

and

$$W_{\text{vis}} \equiv \alpha P_g \frac{R}{v_{\varphi}} \left[ R \frac{\partial}{\partial R} \left( \frac{v_{\varphi}}{R} \right) \right]^2. \quad (5)$$

We assumed the viscosity parameter  $\alpha$  to obtain the gas supply around the disk mid-plane,

$$\alpha = \begin{cases} 0.1 & n > 10^3 \text{ cm}^{-3} \ \& \ T_g < 10^3 \text{ K} \\ 0.0 & \text{otherwise} \end{cases} \quad (6)$$

We consider heating by UV and X-ray (Maloney et al. 1996; Meijerink & Spaans 2005a; Wada 2012) and the optically thin radiative cooling (Meijerink & Spaans 2005b; Wada et al. 2009). We assume that dust grains sublimate above a dust sublimation temperature  $T_{\text{sub}} = 1500$  K. Dust temperature is generally used in local thermal equilibrium with radiation.

We use the public MHD code CANS+ (Matsumoto et al. 2019)<sup>1</sup> with the additional module to evaluate the radiation force and radiative heating/cooling. However, we ignore the magnetic field in the present model. The number of computational cells in each direction is set to  $(N_R, N_z) = (1200, 2304)$ . The cell sizes in the uniform region give high resolutions  $\Delta R = \Delta z = 5 \times 10^{-5}$  pc for  $R < 3.5 \times 10^{-2}$  pc and  $|z| < 3.26 \times 10^{-2}$  pc. On the outside, the cells are stretched to approximately 0.1 pc for a maximum simulation box of  $R = |z| = 50$  pc (Figure 1).

## 2.2. Radiative transfer using CLOUDY

We used density, temperature, and velocities in the central  $r \leq 0.02$  pc in the hydrodynamic simulation described in Section 2.1 (Figure 2), and the data of the 2D cylindrical coordinate were modified for polar grid cells with  $(N_r, N_{\theta}) = (400, 41)$  for  $-30 \leq \theta \leq 30^\circ$ , where  $\theta$  is the angle from the equatorial plane. We then ran the spectral synthesis code CLOUDY (version 17.03) (Ferland et al. 2017).

<sup>1</sup> <https://github.com/chiba-aplab/cansplus>

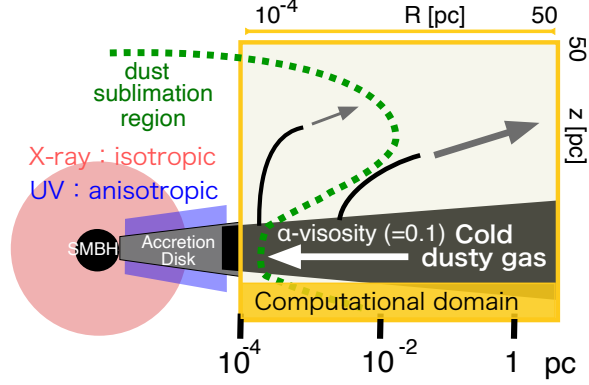


**Figure 1.** Model setup: The central radiation field of anisotropic and isotropic are assumed for UV and X-ray, respectively. Therefore, the dust sublimation region is not spherical (see Paper I in detail). The dusty, cold gas is supplied through the disk and the outflow is launched from the inner most region of the disk ( $r \lesssim 0.1$  pc).  $R_s$  is the Schwarzschild radius.

The SED of the central source was derived from Cloudy’s AGN command and is represented as

$$f(\nu) = \nu^{\alpha_{UV}} \exp(-h\nu/kT_{BB}) \exp(-kT_{IR}/h\nu) \cos i + a\nu^{\alpha_X} \exp(-h\nu/E_1) \exp(-E_2/h\nu), \quad (7)$$

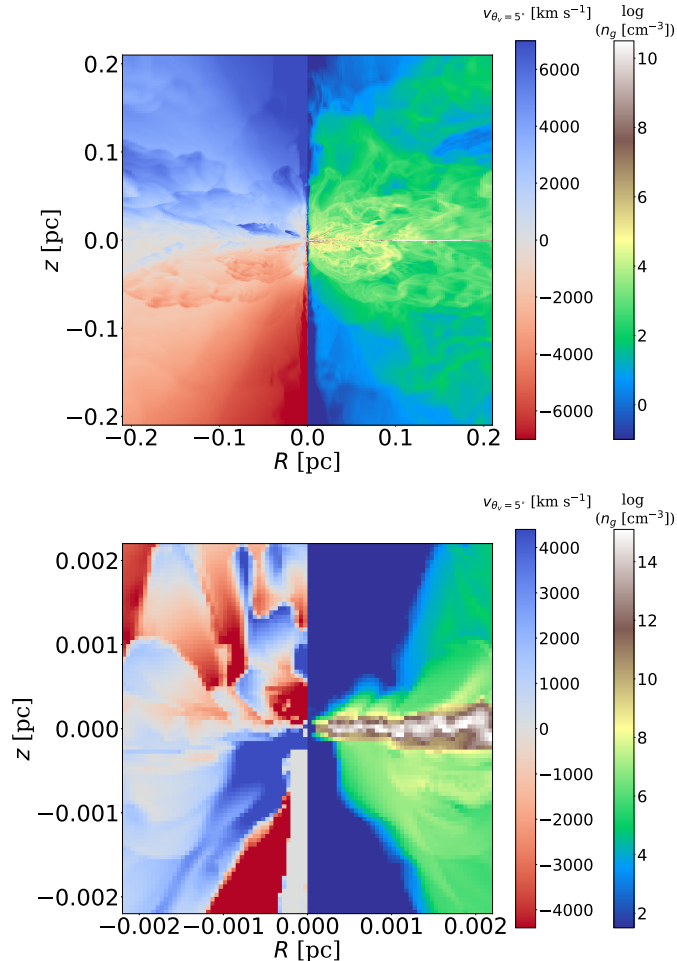
where  $\alpha_{UV} = -0.5$ ,  $T_{BB} = 10^5$  K,  $\alpha_X = -0.7$ ,  $a$  is a constant that yields the X-ray-to-UV ratio  $\alpha_{OX} = -1.4$ ,  $kT_{IR} = 0.01$  Ryd,  $E_1 = 300$  keV,  $E_2 = 0.1$  Ryd, and  $i$  is the angle from the  $z$  axis (i.e., rotational axis). The UV radiation (first term), which derives from the geometrically thin optically thick disk, was assumed to be proportional to  $\cos i$ . By contrast, the X-ray component (second term) was assumed to be isotropic (Figure 1).

We assume that grains are sublimated (i.e., no grains) in the data used in CLOUDY, and the Solar metallicity is assumed. In Paper I, we confirmed that the gas inside  $r \sim 0.01$  pc is mostly dust-free. The following are parts of the input file for CLOUDY:

```

abundances "default.abn" no grains
grains ism function sublimation
filling factor 1.0
no molecules
set nend 2000
set continuum resolution 0.2
    
```

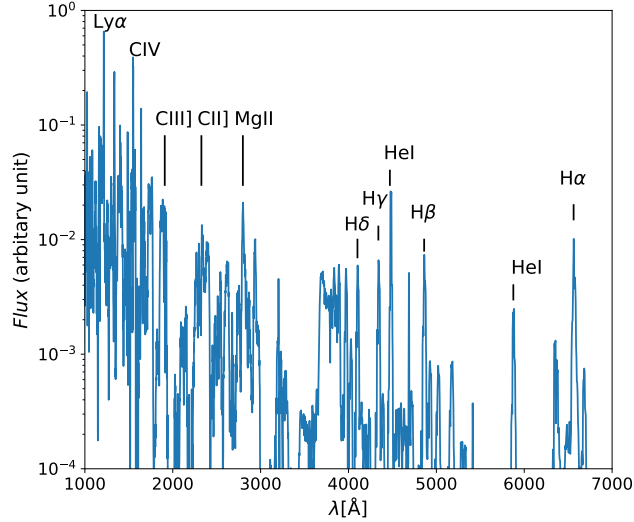
The transmitted SED, calculated using CLOUDY for the inner most cell, was used as an incident SED for the next outward radial cell, and this procedure was repeated up to the outer edge (i.e.,  $r = 0.02$  pc) for a given radial ray (see Wada et al. 2018b, in detail). We confirmed that beyond  $r > 0.02$  pc, most emission lines typically seen in BLRs are very weak.



**Figure 2.** Input radiation-hydrodynamic model, where the top and bottom are the same, but for the central 0.2 pc and 0.002 pc regions, respectively. See also Paper I. The left-half panel shows the line-of-sight velocity for the viewing angle, which is  $5^\circ$  from the rotational axis. The right-half panel shows the number density of the gas. In the gray region near the  $z$  axis, the velocity exceeds  $10^5$  km s $^{-1}$  of the light speed. This region is a temporal structure derived from the numerical artifact near the boundary. However, this high velocity region is not used in the spectrum calculations.

Upon completion of all CLOUDY calculations, we *observed* the system (i.e., all the grid cells within  $r = 0.02$  pc) along the line of sight, assuming the viewing angle  $i$  ( $i = 0$  means face-on). For the azimuthal direction, we assumed that the system was axisymmetric. In addition, the Doppler-shifted emission lines (in which the velocity of each cell was used) from all grid cell spectra were integrated while considering 64 azimuthal directions over  $2\pi$ . This is justified that the optical depth of the prominent lines in CLOUDY calculations are smaller than 0.1, and therefore they are not heavily attenuated by the diffuse media between the observer and the surface of the dense disk, where the most emission lines are originated in. Note that we do not assume optically thin for the radial direction in the CLOUDY calculations.

### 3. RESULTS



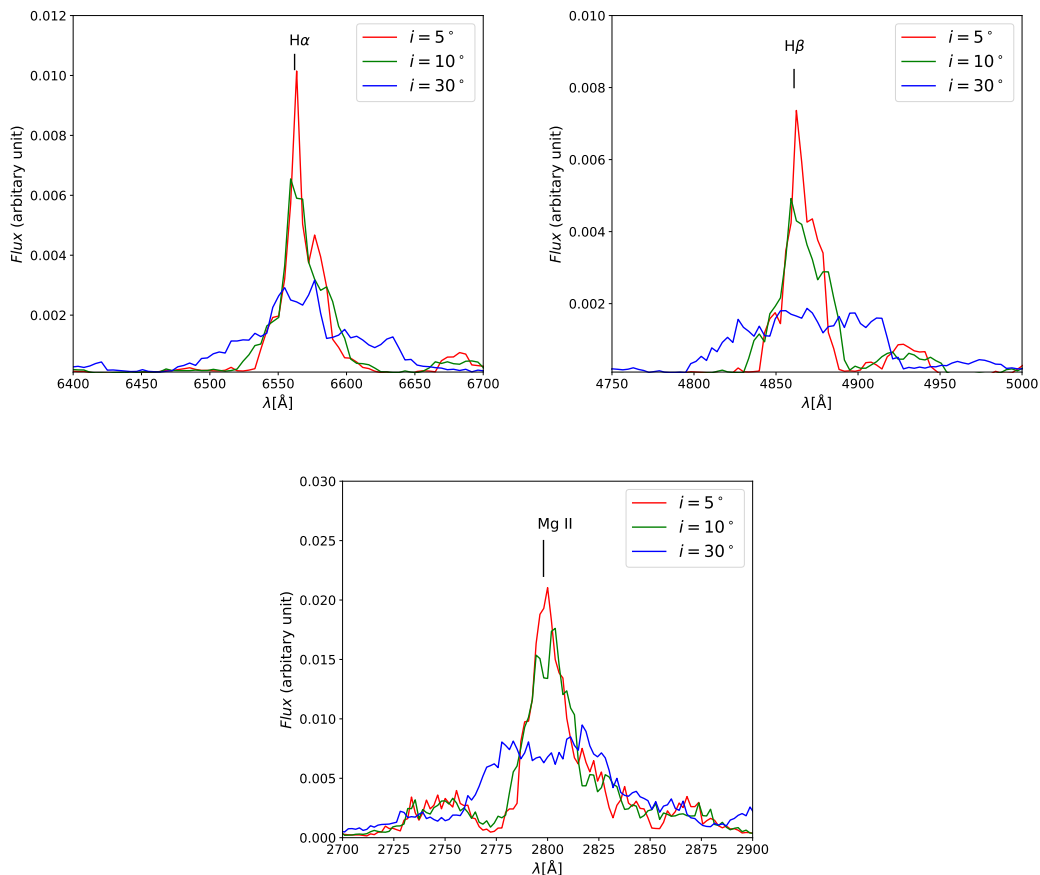
**Figure 3.** Line spectrum calculated using Cloudy between 1000 and 7000 Å. C IV  $\lambda 1549$ , C III ]  $\lambda 1909$ , C II ]  $\lambda 2326$ , Mg II  $\lambda 2798$ , He I  $\lambda 4471$ ,  $\lambda 5876$ , and the hydrogen recombination lines are all marked. The viewing angle is assumed to be  $5^\circ$ .

Figure 3 shows the spectrum between 1000Å and 7000Å, assuming a viewing angle  $i$  of  $5^\circ$  from the rotational axis. Strong hydrogen recombination lines as well as C IV  $\lambda 1549$ , C III ]  $\lambda 1909$ , and Mg II  $\lambda 2798$ , which are often seen in Type 1 and 2 AGNs, are obtained <sup>2</sup>.

Figure 4 shows the spectra that include H $\alpha$ , H $\beta$ , and Mg II. The profiles for all of these lines depend on the viewing angle; it is wider for  $i = 30^\circ$  than  $i = 5^\circ$  or  $10^\circ$ . In H $\alpha$  and Mg II, the line shows a double-peak profile for  $i = 30^\circ$ . This dependence on the viewing angle is a natural consequence in which the emission region for these lines represents the upper or lower surface of the rotating disk, as can be seen in the brownish region of the density map shown in Figure 2 (bottom panel), where  $n \gtrsim 10^{11} \text{ cm}^{-3}$ .

We also observed significant differences in the line profiles of the high-ionization lines (C IV  $\lambda 1549$  and Si IV  $\lambda 1397$ ) as compared with the hydrogen recombination lines and Mg II shown in Figure 4. In Figure 5, C IV shows a double peak profile for  $i = 5^\circ$  and a strong systemic component at the rest-frame wavelength. However, a single peak appears only around the systemic velocity for  $30^\circ$ . Si IV also shows high-velocity components with a systemic component for  $i = 5^\circ$ . For  $i = 30^\circ$ , the profile is a single peak around the systemic component only. Note that the weaker N IV] shows a double-peaked profile for  $i = 30^\circ$ , which is similar to that of Mg II. These results indicate that C IV and Si IV partially originated in the *outflows* located at the upper/lower

<sup>2</sup> It is unclear why the He I  $\lambda 4471$  was stronger than the Balmer lines, which is not usually prominent in observations.



**Figure 4.** Spectra around  $H\alpha$ ,  $H\beta$ , and  $Mg\ II\ \lambda 2798$  for three viewing angles ( $5^\circ$ ,  $10^\circ$  and  $30^\circ$ ).

surface of the disk, which are prominently displayed as the high line-of-sight velocity ( $> 2000\ \text{km s}^{-1}$ ) in the velocity map of the central  $0.002\ \text{pc}$  in Figure 2.

#### 4. DISCUSSION AND CONCLUSION

Since the 1980s, quasar broad emission lines have been known to blue-shift frequently from the systemic velocity, particularly for the high-ionization broad C iv line (e.g., Gaskell 1982; Wilkes & Carswell 1982). This has also been confirmed for Sloan Digital Sky Survey quasars (e.g., Vanden Berk et al. 2001; Richards et al. 2011; Shen et al. 2016). The origin of the velocity shift remains under debate; it could be caused by outflows and osculation by the disk (Gaskell 1982; Chiang & Murray 1996b). However, some observations, including those of velocity-resolved reverberation mapping and line width-time delay relation are not well explained by the disk wind model (Gaskell & Goosmann 2016), which implies that the motion is dominated by gravity (Krolik et al. 1991).

As described in this study, we found that the hydrogen recombination lines and most other emission lines show a wider line profile or double-peaked profiles for larger viewing angles (i.e., closer to edge-on). This is consistent with the notion that BLRs



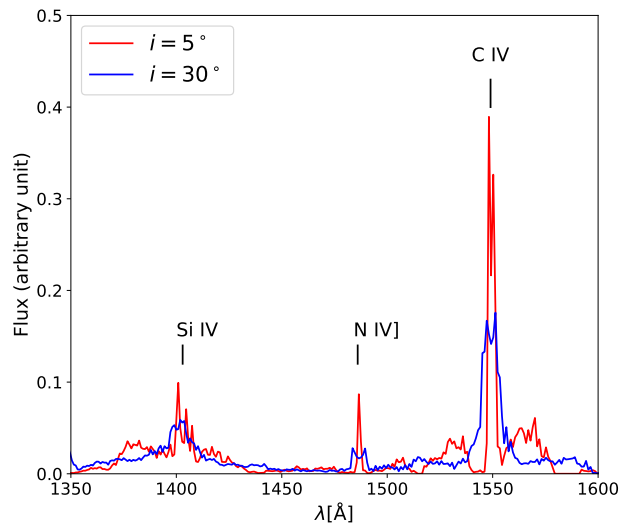


**Figure 5.** Line profiles for three viewing angles ( $5^\circ$  and  $30^\circ$ ): Si IV  $\lambda 1397$ , N IV]  $\lambda 1487$ , C IV  $\lambda 1549$ . The rest-frame wavelengths are shown by vertical lines. Note that blue- and redshifted components appear in both lines for small viewing angles.

originate in the rotating disk (see e.g., [Storchi-Bergmann et al. 2016](#), and references therein). However, our results also show emission lines originating in the radiation-driven wind.

In some disk wind models, two spatially distinct components are required to explain the properties of BLR ([Collin-Souffrin & Lasota 1988](#)). Accordingly, [Yong et al. \(2020\)](#) proposed that the velocity-shift between C IV  $\lambda 1549$  and Mg II  $\lambda 2798$  can be used to infer the orientation of the nucleus. This is basically consistent with what we found in Figure 5<sup>3</sup>. In our present analysis, we assumed that we can observe both far and near sides of the outflows (see Fig. 2). If the far side outflow (i.e., redshifted component) is obscured by the dense disk, we expect that C IV and Si IV are blueshifted with respect to the systemic velocity, or it may show an asymmetric profile.

As [Baldwin et al. \(1995\)](#) indicated in their “locally optimal cloud” representation, the emission line spectrum can be reproduced by integrating various properties of emitting clouds, and the spectra do not necessarily represent physical conditions such as pressure, gas density, or ionization of individual clouds. They also speculated that a chaotic cloud environment could be the source of the lines, and therefore the lines reflect mostly global properties of the clouds. The present results suggest that this rather chaotic depiction is naturally reproduced by the radiation-driven fountain model.

Using the narrow Fe-K $\alpha$  reverberation mapping for a changing-look AGN NGC 3516, [Noda et al. \(2023\)](#) found that the Fe-K emitting radius in the type-2 phase

<sup>3</sup> In the spectra of type-1 AGNs, the Si IV  $\lambda 1397$  line is blended with the O IV]  $\lambda 1402$  line due to their broad nature. However, in typical situations of BLRs (i.e., with the solar or super-solar metallicity), the flux of O IV]  $\lambda 1402$  is less than  $\sim 30\%$  of the total flux of the Si IV + O IV] blend (see, e.g., Figure 29 in [Nagao et al. \(2006\)](#)). Thus we simply write Si IV  $\lambda 1397$  to denote the Si IV + O IV] blend.

is consistent with that of the BLR materials in the type-1 phase. They claimed a possibility that the BLR materials remained at the same location as in the type-1 phase. If the BLR material is mainly originated in the surface of the rotating disk as our results suggested, this observational fact can be naturally understood. However, farther investigation based on the radiation-hydrodynamic simulations by changing the AGN luminosity would be necessary.

## ACKNOWLEDGMENTS

We thank G. Ferland and the CLOUDY team for their regular support. Numerical computations of the radiation-hydrodynamic model were performed on a Cray XC50 at the Center for Computational Astrophysics at the National Astronomical Observatory of Japan and using the Fugaku supercomputer at RIKEN. This work was supported by JSPS KAKENHI Grant Number 21H04496. The work used computational resources of Fugaku provided by RIKEN through the HPCI System Research Project (Project IDs: hp210147, hp210219).

## REFERENCES

- Almeyda, T., Robinson, A., Richmond, M., Nikutta, R., & McDonough, B. 2020, *ApJ*, 891, 26, doi: [10.3847/1538-4357/ab6aa1](https://doi.org/10.3847/1538-4357/ab6aa1)
- Baldwin, J., Ferland, G., Korista, K., & Verner, D. 1995, *ApJL*, 455, L119, doi: [10.1086/309827](https://doi.org/10.1086/309827)
- Barth, A. J., Nguyen, M. L., Malkan, M. A., et al. 2011, *ApJ*, 732, 121, doi: [10.1088/0004-637X/732/2/121](https://doi.org/10.1088/0004-637X/732/2/121)
- Baskin, A., & Laor, A. 2018, *Mon. Not. R. Astron. Soc.*, 474, 1970
- Bentz, M. C., Walsh, J. L., Barth, A. J., et al. 2009, *ApJ*, 705, 199, doi: [10.1088/0004-637X/705/1/199](https://doi.org/10.1088/0004-637X/705/1/199)
- Blandford, R. D., & McKee, C. F. 1982, *ApJ*, 255, 419, doi: [10.1086/159843](https://doi.org/10.1086/159843)
- Buchner, J., Brightman, M., Baloković, M., et al. 2021, *A&A*, 651, A58, doi: [10.1051/0004-6361/201834963](https://doi.org/10.1051/0004-6361/201834963)
- Chiang, J., & Murray, N. 1996a, *ApJ*, 466, 704, doi: [10.1086/177543](https://doi.org/10.1086/177543)
- . 1996b, *ApJ*, 466, 704, doi: [10.1086/177543](https://doi.org/10.1086/177543)
- Collin-Souffrin, S., & Lasota, J.-P. 1988, *PASP*, 100, 1041, doi: [10.1086/132270](https://doi.org/10.1086/132270)
- Czerny, B., & Hryniewicz, K. 2010, <https://arxiv.org/abs/1010.6201>
- Dorodnitsyn, A., & Kallman, T. 2021, *Astrophys. J.*, 910, 67
- Dorodnitsyn, A., Kallman, T., & Bisnovatyi-Kogan, G. S. 2012, *ApJ*, 747, 8, doi: [10.1088/0004-637X/747/1/8](https://doi.org/10.1088/0004-637X/747/1/8)
- Ferland, G. J., & Persson, S. E. 1989, *ApJ*, 347, 656, doi: [10.1086/168156](https://doi.org/10.1086/168156)
- Ferland, G. J., Chatzikos, M., Guzmán, F., et al. 2017, *RMxAA*, 53, 385, <https://arxiv.org/abs/1705.10877>
- Ferrarese, L., & Ford, H. 2005, *SSRv*, 116, 523, doi: [10.1007/s11214-005-3947-6](https://doi.org/10.1007/s11214-005-3947-6)
- Gaskell, C. M. 1982, *ApJ*, 263, 79, doi: [10.1086/160481](https://doi.org/10.1086/160481)
- . 2009, *NewAR*, 53, 140, doi: [10.1016/j.newar.2009.09.006](https://doi.org/10.1016/j.newar.2009.09.006)
- Gaskell, C. M., & Goosmann, R. W. 2016, *Ap&SS*, 361, 67, doi: [10.1007/s10509-015-2648-1](https://doi.org/10.1007/s10509-015-2648-1)
- GRAVITY Collaboration, Sturm, E., Dexter, J., et al. 2018, *Nature*, 563, 657, doi: [10.1038/s41586-018-0731-9](https://doi.org/10.1038/s41586-018-0731-9)

- GRAVITY Collaboration, Amorim, A., Bauböck, M., et al. 2020, *A&A*, 643, A154, doi: [10.1051/0004-6361/202039067](https://doi.org/10.1051/0004-6361/202039067)
- . 2021, *A&A*, 648, A117, doi: [10.1051/0004-6361/202040061](https://doi.org/10.1051/0004-6361/202040061)
- GRAVITY Collaboration, Amorim, A., Bourdarot, G., et al. 2022. <https://arxiv.org/abs/2209.14410>
- Izumi, T., & Wada, K., e. a. 2023, *Science*, submitted
- Izumi, T., Wada, K., Fukushige, R., Hamamura, S., & Kohno, K. 2018, *ApJ*, 867, 48, doi: [10.3847/1538-4357/aae20b](https://doi.org/10.3847/1538-4357/aae20b)
- Krolik, J. H., Horne, K., Kallman, T. R., et al. 1991, *ApJ*, 371, 541, doi: [10.1086/169918](https://doi.org/10.1086/169918)
- Kudoh, Y., Wada, K., Kawakatu, N., & Nomura, M. 2023, *ApJ*, submitted (Paper I)
- Lawther, D., Goad, M. R., Korista, K. T., Ulrich, O., & Vestergaard, M. 2018, *MNRAS*, 481, 533, doi: [10.1093/mnras/sty2242](https://doi.org/10.1093/mnras/sty2242)
- Maloney, P. R., Hollenbach, D. J., & Tielens, A. G. G. M. 1996, *ApJ*, 466, 561, doi: [10.1086/177532](https://doi.org/10.1086/177532)
- Matsumoto, K., Nakagawa, T., Wada, K., et al. 2022, *ApJ*, 934, 25, doi: [10.3847/1538-4357/ac755f](https://doi.org/10.3847/1538-4357/ac755f)
- Matsumoto, Y., Asahina, Y., Kudoh, Y., et al. 2019, *PASJ*, 71, 83, doi: [10.1093/pasj/psz064](https://doi.org/10.1093/pasj/psz064)
- Matthews, J. H., Knigge, C., Higginbottom, N., et al. 2020, *Mon. Not. R. Astron. Soc.*, 492, 5540
- Meijerink, R., & Spaans, M. 2005a, *A&A*, 436, 397, doi: [10.1051/0004-6361:20042398](https://doi.org/10.1051/0004-6361:20042398)
- . 2005b, *A&A*, 436, 397, doi: [10.1051/0004-6361:20042398](https://doi.org/10.1051/0004-6361:20042398)
- Naddaf, M.-H., Czerny, B., & Szczerba, R. 2021, *Astrophys. J.*, 920, 30
- Nagao, T., Marconi, A., & Maiolino, R. 2006, *A&A*, 447, 157, doi: [10.1051/0004-6361:20054024](https://doi.org/10.1051/0004-6361:20054024)
- Namekata, D., & Umemura, M. 2016, *MNRAS*, 460, 980, doi: [10.1093/mnras/stw862](https://doi.org/10.1093/mnras/stw862)
- Netzer, H. 2013, *The Physics and Evolution of Active Galactic Nuclei*
- . 2015, *ARA&A*, 53, 365, doi: [10.1146/annurev-astro-082214-122302](https://doi.org/10.1146/annurev-astro-082214-122302)
- Netzer, H. 2020, *Mon. Not. R. Astron. Soc.*, 494, 1611
- Netzer, H., & Laor, A. 1993, *ApJL*, 404, L51, doi: [10.1086/186741](https://doi.org/10.1086/186741)
- Noda, H., Mineta, T., Minezaki, T., et al. 2023, *ApJ*, 943, 63, doi: [10.3847/1538-4357/aca963](https://doi.org/10.3847/1538-4357/aca963)
- Ogawa, S., Ueda, Y., Wada, K., & Mizumoto, M. 2022, *ApJ*, 925, 55, doi: [10.3847/1538-4357/ac3cb9](https://doi.org/10.3847/1538-4357/ac3cb9)
- Ohsuga, K., Mori, M., Nakamoto, T., & Mineshige, S. 2005, *ApJ*, 628, 368, doi: [10.1086/430728](https://doi.org/10.1086/430728)
- Osterbrock, D. E., & Ferland, G. J. 2006, *Astrophysics of gaseous nebulae and active galactic nuclei*
- Osterbrock, D. E., & Mathews, W. G. 1986, *ARA&A*, 24, 171, doi: [10.1146/annurev.aa.24.090186.001131](https://doi.org/10.1146/annurev.aa.24.090186.001131)
- Peterson, B. M. 1997, *An Introduction to Active Galactic Nuclei* (Cambridge University Press), doi: [10.1017/CBO9781139170901](https://doi.org/10.1017/CBO9781139170901)
- Peterson, B. M., Ali, B., Horne, K., et al. 1993, *ApJ*, 402, 469, doi: [10.1086/172150](https://doi.org/10.1086/172150)
- Peterson, B. M., Ferrarese, L., Gilbert, K. M., et al. 2004, *ApJ*, 613, 682, doi: [10.1086/423269](https://doi.org/10.1086/423269)
- Richards, G. T., Kruczek, N. E., Gallagher, S. C., et al. 2011, *AJ*, 141, 167, doi: [10.1088/0004-6256/141/5/167](https://doi.org/10.1088/0004-6256/141/5/167)
- Schartmann, M., Wada, K., Prieto, M. A., Burkert, A., & Tristram, K. R. W. 2014, *MNRAS*, 445, 3878, doi: [10.1093/mnras/stu2020](https://doi.org/10.1093/mnras/stu2020)
- Shakura, N. I., & Sunyaev, R. A. 1973, *A&A*, 24, 337
- Shen, Y., Brandt, W. N., Richards, G. T., et al. 2016, *ApJ*, 831, 7, doi: [10.3847/0004-637X/831/1/7](https://doi.org/10.3847/0004-637X/831/1/7)
- Smith, M. D., & Raine, D. J. 1985, *MNRAS*, 212, 425, doi: [10.1093/mnras/212.2.425](https://doi.org/10.1093/mnras/212.2.425)

- Storchi-Bergmann, T., Schimoia, J. S., Peterson, B. M., et al. 2016.  
<https://arxiv.org/abs/1612.06843>
- Suganuma, M., Yoshii, Y., Kobayashi, Y., et al. 2006, *ApJ*, 639, 46,  
doi: [10.1086/499326](https://doi.org/10.1086/499326)
- Uzuo, T., Wada, K., Izumi, T., et al. 2021, *ApJ*, 915, 89,  
doi: [10.3847/1538-4357/ac013d](https://doi.org/10.3847/1538-4357/ac013d)
- Vanden Berk, D. E., Richards, G. T., Bauer, A., et al. 2001, *AJ*, 122, 549,  
doi: [10.1086/321167](https://doi.org/10.1086/321167)
- Wada, K. 2012, *The Astrophysical Journal*, 758, 66
- . 2015, *The Astrophysical Journal*, 812, 82
- Wada, K., Fukushige, R., Izumi, T., & Tomisaka, K. 2018a, *ApJ*, 852, 88,  
doi: [10.3847/1538-4357/aa9e53](https://doi.org/10.3847/1538-4357/aa9e53)
- Wada, K., Papadopoulos, P. P., & Spaans, M. 2009, *ApJ*, 702, 63,  
doi: [10.1088/0004-637X/702/1/63](https://doi.org/10.1088/0004-637X/702/1/63)
- Wada, K., Yonekura, K., & Nagao, T. 2018b, *ApJ*, 867, 49,  
doi: [10.3847/1538-4357/aae204](https://doi.org/10.3847/1538-4357/aae204)
- Wilkes, B. J., & Carswell, R. F. 1982, *MNRAS*, 201, 645,  
doi: [10.1093/mnras/201.3.645](https://doi.org/10.1093/mnras/201.3.645)
- Williams, P. R., Pancoast, A., Treu, T., et al. 2020, *Astrophys. J.*, 902, 74
- Williamson, D., Hönig, S., & Venanzi, M. 2020, *ApJ*, 897, 26,  
doi: [10.3847/1538-4357/ab989e](https://doi.org/10.3847/1538-4357/ab989e)
- Yong, S. Y., Webster, R. L., King, A. L., et al. 2020, *MNRAS*, 491, 1320,  
doi: [10.1093/mnras/stz3074](https://doi.org/10.1093/mnras/stz3074)